Inorganic Chemistry

ARTICLE

pubs.acs.org/IC

Modulating Magnetic Dynamics of Three Dy_2 Complexes through Keto−Enol Tautomerism of the *o*-Vanillin Picolinoylhydrazone Ligand

Yun-Nan Guo,[†,‡] Xiao-Hua Chen,[§] Shufang Xue,[†,‡] and Jinkui Tang*[,†]

[†]State Key Laboratory of Rare Earth Resource Utilization, Changchun Institute of Applied Chemistry, Chinese Academy of Sciences, Changchun 130022, People's Republic of China

[‡]Graduate School of the Chinese Academy of Sciences, Beijing 100039, People's Republic of China

[§]College of Chemistry and Materials Science, Fujian Normal University, Fuzhou, 350007, People's Republic of China

Supporting Information

ABSTRACT: Complexation of dysprosium(III) with the heterodonor chelating ligand *o*-vanillin picolinoylhydrazone (H_2**ovph**) in the presence of different bases affords three new dinuclear dysprosium(III) coordination compounds, namely, $[Dy_2(\mathbf{ovph})_2(NO_3)_2(H_2O)_2]\cdot 2H_2O$ (**1**), $[Dy_2(\mathbf{Hovph})(\mathbf{ovph})(NO_3)_2(H_2O)_4]\cdot NO_3\cdot 2CH_3OH\cdot 3H_2O$ (**2**), and $Na[Dy_2(\mathbf{Hovph})_2(\mu_2\text{-}OH)(OH)(H_2O)_5]\cdot 3Cl\cdot 3H_2O$ (**3**), where the aroylhydrazone ligand adopts different coordination modes in respective structures depending on the reaction conditions, as revealed by single-crystal X-ray analyses to be due to their tautomeric maneuver. The magnetic properties of **1**−**3** are drastically distinct. Compounds **1** and **2** show single-molecule-magnet behavior, while no out-of-phase alternating-current signal is noticed for **3**. The structural differences induced by the different coordinate fashions of the ligand may influence the strength of the local crystal field, the magnetic interactions between metal centers, and the local tensor of anisotropy on each Dy site and their relative orientations, therefore generating dissimilar dynamic magnetic behavior.

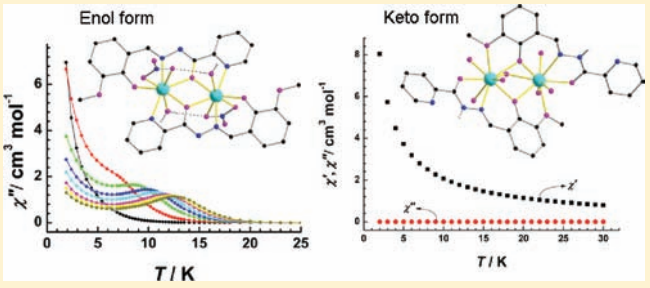

INTRODUCTION

Single-molecule magnets (SMMs)[1−3] have attracted increasing attention of both physicists and chemists because of their potential applications for use in high-density magnetic memories,[4,5] quantum computing devices,[6,7] and molecular spintronics.[8,9] Whereas attention was initially focused on coordination clusters containing 3d metal ions,[10] significant attention is now being paid to incorporating 4f ions into SMMs in either mixed 3d/4f or pure 4f clusters.[11−13] The use of the heavy lanthanide ions, such as terbium(III),[14−16] dysprosium(III),[11,17] holmium(III),[18] and erbium(III)[19−21] is one of the most promising ways to design high-barrier SMMs as a result of their significant magnetic anisotropy arising from the large, unquenched orbital angular momentum. It is now well-established that mononuclear lanthanide complexes may behave as SMMs, when their coordination environment results in highly anisotropic situations.[17] In addition to these monometallic systems, polymetallic lanthanide clusters can also exhibit SMM properties, most of them containing dysprosium(III) with different topologies. Such compounds exhibiting large observed relaxation barriers[22−27] advance the prospects of SMMs, potentially bringing the goals of molecule-based information storage and processing closer to reality.[28] Other dysprosium(III) complexes are interesting for their very fascinating physics, such as spin chirality[29−31] and multiple relaxation pathways.[24,28,32]

Ligand design is one of the key components for achieving pure dysprosium-based systems with tailor-made properties. To understand how the magnetic anisotropy of 4f ions directs the SMM properties of multinuclear compounds, it is helpful to focus on lower-nuclearity clusters.[33] Selection of organic ligands formed by reaction between the *o*-vanillin and hydrazine derivatives is a good choice to construct such clusters, as we and others have recently demonstrated (Scheme 1),[22−24] for the following two reasons: (1) This kind of multidentate ligand has both two or more oxygen donors and two or more nitrogen donors. These donors with suitable relative positions in the ligand can coordinate to several metal centers.[34] (2) The *o*-vanillin group displays a variety of bonding geometries, such as monodentate, bidentate bridging, and chelate bridging.[35,36]

In this context, we decided to explore the possibility of constructing new magnetically interesting molecules using *o*-vanillin picolinoylhydrazone (H_2**ovph**; Scheme 1d) as such a versatile ligand. We report herein the synthesis, structures, and magnetic properties of three dinuclear dysprosium(III) complexes, $[Dy_2(\mathbf{ovph})_2(NO_3)_2(H_2O)_2]\cdot 2H_2O$ (**1**), $[Dy_2(\mathbf{Hovph})(\mathbf{ovph})(NO_3)_2(H_2O)_4]\cdot NO_3\cdot 2CH_3OH\cdot 3H_2O$ (**2**), and $Na[Dy_2(\mathbf{Hovph})_2(\mu_2{-}OH)(OH)(H_2O)_5]\cdot 3Cl\cdot 3H_2O$ (**3**), assembled from dysprosium salts and the H_2**ovph** ligand. Of particular interest in the present study is the clear realization, as revealed by crystallographical and IR spectral investigations, of the tautomeric

Received: July 14, 2011
Published: September 08, 2011

   dx.doi.org/10.1021/ic2014978 | *Inorg. Chem.* 2011, 50, 9705–9713

maneuver of the aroylhydrazone ligand, producing three novel complexes with different coordination modes (Scheme 2), depending on the reaction conditions. The structural differences induced by the different coordinate fashions of the ligand are mostly responsible for the distinct relaxation dynamics observed; namely, compounds **1** and **2** show SMM behavior, while no out-of-phase alternating-current (ac) signal is noticed for **3**.

EXPERIMENTAL SECTION

General Procedures. All chemicals were used as commercially obtained without further purification. Elemental analyses for carbon, hydrogen, and nitrogen were carried out on a Perkin-Elmer 2400 analyzer. Fourier transform IR (FTIR) spectra were recorded with a Perkin-Elmer FTIR spectrophotometer using the reflectance technique (4000−300 cm^{-1}). Samples were prepared as KBr disks. All magnetization data were recorded on a Quantum Design MPMS-XL7 SQUID magnetometer. The variable-temperature magnetization was measured with an external magnetic field of 1000 Oe in the temperature range of 1.9−300 K. Samples were restrained in eicosane to prevent torquing. The experimental magnetic susceptibility data are corrected for the diamagnetism estimated from Pascal's tables and sample holder calibration.

Scheme 1. Title Ligand H_2ovph, the Related Ligands (H_3L_1,[24] H_2L_2,[23] and H_2L_3[22]), and Their Coordinating Modes in Dysprosium(III)-Based SMMs

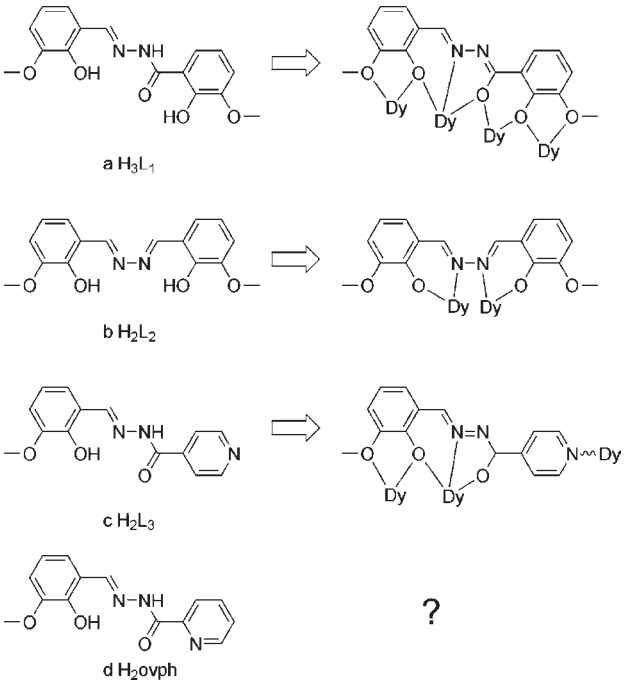

X-ray Crystallography. Single-crystal X-ray diffraction measurements of the title complexes were carried out on a SMART CCD area detector equipped with a graphite crystal monochromator situated in the incident beam for data collection at 191(2) K. The structures were solved by direct methods and refined with full-matrix least-squares techniques using *SHELXS-97* and *SHELXL-97* programs.[37] Anisotropic thermal parameters were assigned to all non-hydrogen atoms. The hydrogen atoms were introduced in calculated positions and refined with a fixed geometry with respect to their carrier atoms. CCDC 830671 (**1**), 830672 (**2**), and 830673 (**3**) contain the supplementary crystallographic data for this paper. These data can be obtained free of charge from the Cambridge Crystallographic Data Centre via www.ccdc.cam.ac.uk/data_request/cif.

Synthesis of H_2ovph. The Schiff-base ligand H_2**ovph** is synthesized by condensation of picolinoyl hydrazide and *o*-vanillin in a 1:1 ratio in methanol using the reported procedure.[38]

Synthesis of $[Dy_2(ovph)_2(NO_3)_2(H_2O)_2]\cdot 2H_2O$ (1). A solution of $Dy(NO_3)_3\cdot 6H_2O$ (0.2 mmol, 91.32 mg) and H_2**ovph** (0.2 mmol, 54.26 mg) in a mixed solvent of methanol (5 mL) and acetonitrile (10 mL) was stirred for 5 min. Then Et_3N (0.2 mmol) was added, and the mixture was stirred for 3 h. The resultant yellow solution was left unperturbed to allow for slow evaporation of the solvent. Yellow single crystals, suitable for X-ray diffraction analysis, were formed after 1 month. Yield: 38 mg (36%, based on the metal salt). Elem anal. Calcd for $C_{28}H_{30}N_8O_{16}Dy_2$: C, 31.71; H, 2.83; N, 10.57. Found: C, 31.60; H, 2.62; N, 10.39. IR (KBr, cm^{-1}): 3392(br), 2993(w), 2842(w), 1599(s), 1557(s), 1541(w), 1517(m), 1479(s), 1465(w), 1440(m), 1383(s), 1340(s), 1303(m), 1281(m), 1248(m), 1215(m), 1170(w), 1155(s), 1083(m), 1055(w), 1021(w), 966(w), 922(w), 859(w), 813(w), 802(w), 749(m), 715(w), 691(m), 639(m), 580(w).

Synthesis of $[Dy_2(Hovph)(ovph)(NO_3)_2(H_2O)_4]\cdot NO_3\cdot 2CH_3OH\cdot 3H_2O$ (2). A procedure similar to that for **1** was followed except that Et_3N was replaced by pyridine (1.0 mmol, 0.08 mL). Yield: 42 mg (34%, based on the metal salt). Elem anal. Calcd for $C_{30}H_{45}N_9O_{24}Dy_2$: C, 29.01; H, 3.63; N, 10.16. Found: C, 28.59; H, 3.54; N, 10.02. IR (KBr, cm^{-1}): 3349(br), 3235(w), 2839(w), 1624(w), 1610(s), 1591(w), 1561(s), 1546(w), 1477(w), 1465(m), 1436(m), 1333(w), 1307(m), 1287(m), 1241(m), 1219(s), 1173(w), 1161(w), 1090(w), 1054(w), 1021(w),

Scheme 2. Reversible Deprotonation and Base-Assisted Keto−Enol Tautomerism of H_2ovph and the Corresponding Coordination Modes in Complexes 1−3

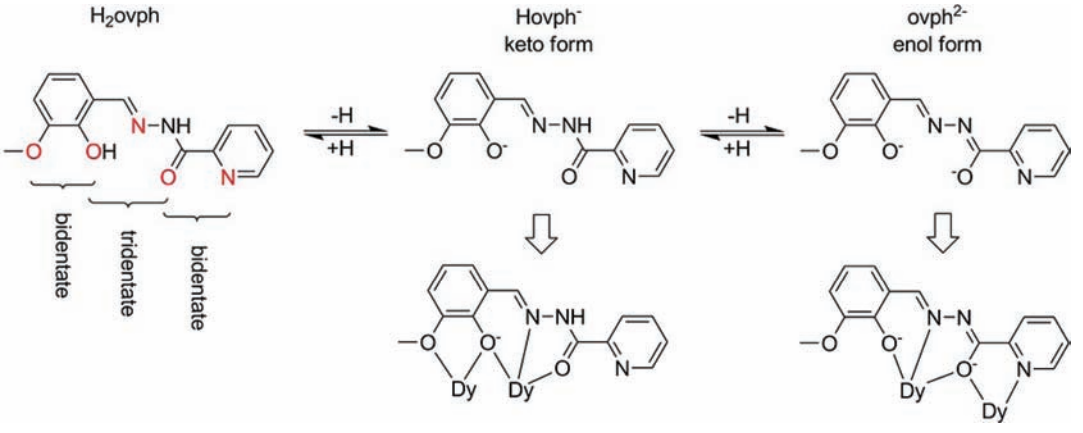

965(w), 921(w), 863(w), 812(w), 789(w), 745(m), 713(w), 697(m), 637(m), 584(w).

Synthesis of $Na[Dy_2(Hovph)_2(\mu_2\text{-}OH)(OH)(H_2O)_5]\cdot 3Cl\cdot 3H_2O$ (3). $DyCl_3\cdot 6H_2O$ (0.2 mmol, 75.4 mg) and H_2ovph (0.2 mmol, 54.26 mg) in a mixed solvent of methanol (5 mL) and acetonitrile (10 mL) was stirred for 5 min and gradually formed a red solution. Then 0.3 mL of methanolic solution of NaN_3 (0.1 mmol) was added to the reaction mixture, and the mixture was stirred for 3 h. The resultant yellow solution was left unperturbed to allow for slow evaporation of the solvent. Yellow single crystals, suitable for X-ray diffraction analysis, were formed after 1 month. Yield: 49 mg (41%, based on the metal salt). Elem anal. Calcd for $C_{28}H_{44}Cl_3N_6O_{17}Dy_2Na$: C, 28.21; H, 3.69; N, 7.05. Found: C, 27.97; H, 3.51; N, 6.95. IR (KBr, cm^{-1}): 3205(br), 1618(s), 1588(s), 1566(s), 1458(s), 1438(w), 1279(m), 1245(s), 1220(s), 1167(w), 1113(w), 1090(m), 1066(w), 961(w), 915(w), 815(w), 786(w), 739(m), 713(w), 698(m), 643(m), 622(w), 527(w), 482(w).

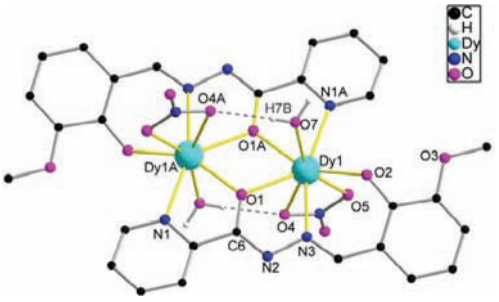

Figure 1. Molecular structure of complex **1**. Organic hydrogen atoms and lattice water are omitted for clarity.

RESULTS AND DISCUSSION

Crystal Structure of 1. The reaction of $Dy(NO_3)_3\cdot 6H_2O$ with H_2**ovph** in methanol/acetonitrile in the presence of Et_3N produces yellow crystals of **1** after 1 month. Single-crystal X-ray studies revealed that **1** crystallizes in the triclinic space group $P\bar{1}$. A perspective view of the molecular structure of **1** is represented in Figure 1. Details for the structure solution and refinement are summarized in Table 1, and selected bond distances and angles are listed in Tables 2 and 3. A structural study of **1** showed it to be a dinuclear *trans*-dysprosium(III) complex. Two **ovph**$^{2-}$ ligands coordinate two dysprosium centers in an antiparallel or "head-to-tail" fashion with the tridentate unit (O1, N3, and O2) and the bidentate picolinoyl group (O1 and N1) (Scheme 2). Carbonyl oxygen atoms (O1 and O1A) of the ligands bind in their conjugate deprotonated enol form (O^-) with a C6−O1 distance of 1.306(7) Å (Table 2) and bridge the two metal centers, giving rise to a four-membered Dy_2O_2 rhomb, which exhibits a center of symmetry with a Dy···Dy distance of 3.8258(6) Å and two

Table 2. Selected Bond Distances (Å) for H_2ovph in Complexes 1−3

	1	2	3
C6−N2	1.308(8)	1.315(10)	1.325(9)
C6−O1	1.306(7)	1.297(10)	1.254(8)
C20−N5		1.323(11)	1.329(8)
C20−O4		1.240(10)	1.232(8)

Table 1. Crystallographic Data and Structure Refinement for Complexes 1−3

	1	2	3
formula	$C_{28}H_{30}Dy_2N_8O_{16}$	$C_{30}H_{45}Dy_2N_9O_{24}$	$C_{28}H_{44}Cl_3Dy_2N_6NaO_{17}$
M_r	1059.60	1240.75	1191.03
cryst size [mm]	0.22 × 19 × 0.17	0.25 × 0.22 × 0.20	0.25 × 0.21 × 0.18
color	yellow blocks	yellow blocks	yellow blocks
cryst syst	triclinic	orthorhombic	triclinic
space group	$P\bar{1}$	$P2_12_12_1$	$P\bar{1}$
T [K]	191(2)	191(2)	191(2)
a [Å]	9.3234(8)	10.335(2)	8.5593(4)
b [Å]	9.4773(9)	16.368(3)	15.5490(8)
c [Å]	11.4313(10)	27.235(5)	15.5897(8)
α [deg]	69.1140(10)	90	85.7660(10)
β [deg]	83.773(2)	90	83.7050(10)
γ [deg]	66.6130(10)	90	82.6390(10)
V [Å^3]	865.53(13)	4607.3(16)	2041.54(18)
Z	1	4	2
D_{calcd} [g cm^{-3}]	2.033	1.789	1.938
μ(Mo Kα) [mm^{-1}]	0.71073	0.71073	0.71073
F(000)	514	2448	1168
reflns collected	4825	25 708	11 450
unique reflns	3393	9016	7989
R_{int}	0.0243	0.0620	0.0228
param/restraints	256/6	557/2	514/0
GOF	1.076	1.011	1.052
R1 [$I > 2\sigma(I)$]	0.0380	0.0443	0.0404
wR2 (all data)	0.0917	0.1038	0.1079
largest diff peak/hole [e Å^{-3}]	1.782/−0.842	1.233/−0.819	3.351/−1.445

dx.doi.org/10.1021/ic2014978 |*Inorg. Chem.* 2011, 50, 9705–9713

Dy−O−Dy angles of 110.12(16)°. In addition, one nitrate (O4 and O5) and one water molecule (O7) are coordinating to each dysprosium ion, leading to a coordination number of 8, which exhibits a hula-hoop-like geometry whose cyclic ring (hula hoop) is shaped by the stereochemical preferences of two **ovph**$^{2-}$ ligands (O1, N3, O2, O1A, and N1A, as shown in Figures 1 and S1 in the Supporting Information).[39,40]

Table 3. Selected Bond Distances (Å) and Angles (deg) in Complexes 1−3[a]

Compound **1**			
Dy1−O1	2.319(4)	Dy1−O1A	2.348(4)
Dy1−O2	2.179(4)	Dy1−O4	2.462(5)
Dy1−O5	2.451(5)	Dy1−O7	2.363(5)
Dy1−N1A	2.477(5)	Dy1−N3	2.453(5)
Dy1···Dy1A	3.8258(6)	Dy1−O1−Dy1A	110.12(16)
Compound **2**			
Dy1−O1	2.320(5)	Dy1−O2	2.189(6)
Dy1−O5	2.425(5)	Dy1−O6	2.509(5)
Dy1−O7	2.513(6)	Dy1−O8	2.581(6)
Dy1−O10	2.405(6)	Dy1−O11	2.402(6)
Dy1−N3	2.495(7)	Dy2−O1	2.334(5)
Dy2−O4	2.322(6)	Dy2−O5	2.295(6)
Dy2−O12	2.473(6)	Dy2−O13	2.563(6)
Dy2−O15	2.407(6)	Dy2−O16	2.391(6)
Dy2−N1	2.532(7)	Dy2−N6	2.539(8)
Dy1···Dy2	3.8926(8)	Dy1−O5−Dy2	111.1(2)
Dy1−O1−Dy2	113.5(2)		
Compound **3**			
Dy1−O1	2.357(4)	Dy1−O2	2.321(4)
Dy1−O5	2.401(4)	Dy1−O6	2.482(4)
Dy1−O7	2.393(5)	Dy1−O8	2.396(5)
Dy1−O9	2.417(5)	Dy1−O14	2.528(4)
Dy1−N3	2.543(6)	Dy2−O2	2.406(4)
Dy2−O3	2.504(4)	Dy2−O4	2.330(4)
Dy2−O5	2.314(4)	Dy2−O10	2.422(4)
Dy2−O11	2.417(4)	Dy2−O12	2.467(5)
Dy1−O14	2.490(4)	Dy2−N6	2.516(5)
Dy1···Dy2	3.6145(4)	Dy1−O2−Dy2	99.72(16)
Dy1−O5−Dy2	100.08(15)	Dy1−O14−Dy2	92.14(15)

[a] Symmetry code for **1**: A, $-x+1, -y+1, -z+1$.

The coordinated water molecule (O7) binds to the neighboring nitrate via an intramolecular hydrogen bond O4[a]···H7B−O7 (symmetry code: a, $-x+1, -y+1, -z+1$; Figure 1). Every Dy_2 molecule connects to six lattice water molecules, as shown in Figure 2, left. Meanwhile, each lattice water (O1w) acts as a hydrogen-bonding connector, joining three Dy_2 units via strong O1w−H1wA···N2[a], O7−H7C···O1w[b], and O1w−H1wB···O2[c] bonds (symmetry codes: b, $-x+1, -y+2, -z+1$; c, $x+1, y, z$; see Table S1 in the Supporting Information for details and the red circle in Figure 2, right), and, thus, a 2D supramolecular motif in **1** is afforded, running along the *ab* plane (Figure 2, right).

Crystal Structure of 2. A procedure similar to that for **1** except that Et_3N was replaced by pyridine yields yellow crystals of **2** after 3 weeks. The single-crystal X-ray structure of the dinuclear **2** is depicted in Figure 3. Compound **2** crystallizes in the space group $P2_12_12_1$, with $Z = 4$. The molecule occupies a general site, in which two ligands coordinate two dysprosium centers in a parallel fashion, leading to a noncentrosymmetric $Dy_2(\mu\text{-}O)_2$ core with a Dy···Dy distance of 3.8926(8) Å and two Dy−O−Dy angles of 113.5(2)° and 111.1(2)°. Close inspection of the bond distances reveals that one of the ligands has undergone keto−enol tautomerism (Scheme 1 and Table 2). A comparison of the bond distances in complex **2** shows considerable differences between the two tautomeric forms of the ligand (Table 2). The C20−O4 bonds in the keto form [1.240(10) Å] are shorter than the corresponding bonds C6−O1 in the enolate form [1.297(10) Å], congruent with the chemical structures of both forms (Scheme 1). Therefore, in the dideprotonated **ovph**$^{2-}$ ligand, O1 as an alkoxido atom (O^-) bridges the two metal centers, similar to that in complex **1**. However, the monodeprotonated **Hovph**$^-$ ligand coordinates two dysprosium centers with the tridentate unit (O4, N6, and O5) and the bidentate *o*-vanillin group (O5 and O6), in which the aroylhydrazone part keeps the original keto state.[41] The coordination spheres of Dy1 and Dy2 are each completed by two water molecules and one nitrate ligand, making them nine-coordinate with a monocapped square-antiprismatic geometry (Figure S1 in the Supporting Information).

Crystal Structure of 3. The reaction of $DyCl_3 \cdot 6H_2O$ with H_2**ovph** in methanol/acetonitrile, in the presence of NaN_3, produces yellow crystals of **3**, whose molecular structure determined by single-crystal X-ray diffraction is depicted in Figure 4. Compound **3** crystallizes in the space group $P\bar{1}$, with $Z = 2$. Evidently,

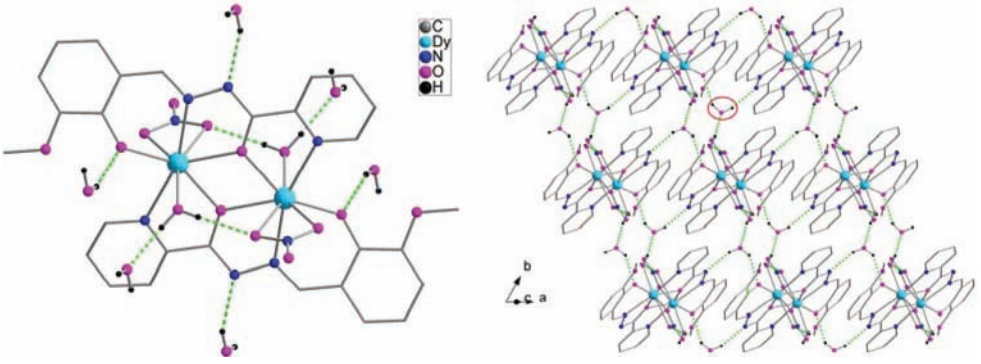

Figure 2. (left) Hydrogen bonding between the Dy_2 unit and six peripheral lattice water molecules. (right) 2D supramolecular plane of **1**. The red circle highlights where a lattice water joins three Dy_2 units.

dx.doi.org/10.1021/ic2014978 |*Inorg. Chem.* 2011, 50, 9705–9713

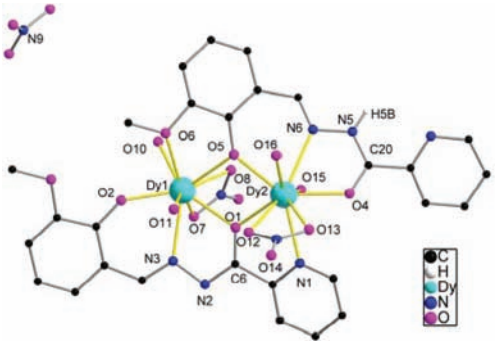

Figure 3. Molecular structure of complex **2**. Hydrogen atoms and lattice solvent molecules are omitted for clarity.

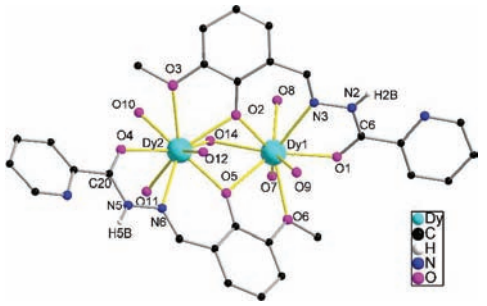

Figure 4. Dinuclear unit of **3**. Hydrogen atoms are omitted for clarity.

in the presence of a weak base (N_3^-), both of the aroylhydrazone ligands remained in the keto form (Scheme 2 and Table 2). Two H**ovph**$^-$ ligands coordinate Dy1 and Dy2 centers in an antiparallel fashion with their tridentate unit and bidentate *o*-vanillin group. Different from **1** and **2**, complex **3** exhibits a $Dy_2(\mu\text{-}O)_3$ core, which is created by the phenoxido groups (O2 and O5) of two H**ovph**$^-$ ligands and one additional μ_2-hydroxido (O14) bridge with a Dy···Dy distance of 3.6145(4) Å and three Dy−O−Dy angles of 99.72 (16)°, 100.08(15)°, and 92.14(15)°. The coordination spheres of Dy1 and Dy2 are completed by five water molecules (O8−O12) and one OH^- ligand (O7), making them nine-coordinate with a distorted monocapped square-antiprismatic geometry (Figure S1 in the Supporting Information). Along with coordination on Dy1, O7 and O9 also bridge Na1 ions below and above the Dy_2 molecule (Figure S2 in the Supporting Information). The band distances of Dy1−O7 [2.393(5) Å] and Dy1−O9 [2.417(5) Å] are corresponding to one OH^- ligand and one water molecule, respectively.

IR Spectra. The IR spectrum of the ligand exhibits a band at 3273 cm^{-1} due to ν(NH) stretches, indicative of its ketonic nature in the solid state, which was also observed in complexes **2** (3235 cm^{-1}) and **3** (3205 cm^{-1}). The absence of the ν(NH) band in the IR spectrum of complex **1** is consistent with enolization.[38]

The ν(C═O) absorption at 1650−1700 cm^{-1} in the spectrum of the free hydrazone is observed at 1618 and 1624 cm^{-1} in complexes **2** and **3**, respectively, in accordance with coordination through the carbonyl oxygen (Figure 5).[42] In complex **1**, no absorption attributable to ν(C═O) was observed, further indicating full deprotonation of H_2**ovph** in **1**.

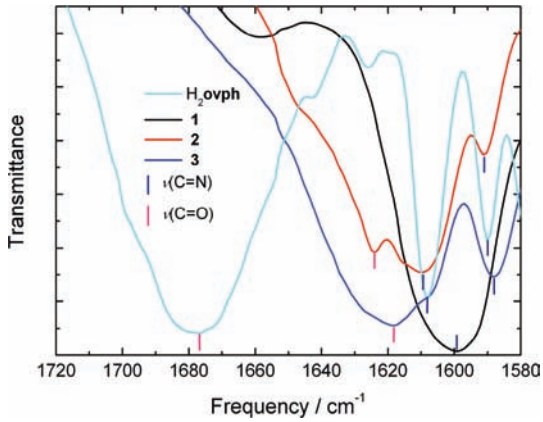

Figure 5. IR spectra of a crystalline sample of H_2**ovph** and complexes **1**−**3** with ν(C═N) modes (blue vertical bar) and ν(C═O) modes (red vertical bar).

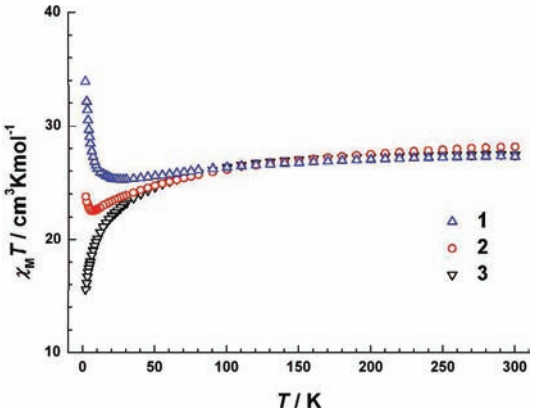

Figure 6. Temperature dependence of the $\chi_M T$ products at 1 kOe for **1**−**3**.

The ν(C═N) vibration modes at 1590 and 1608 cm^{-1} in the spectrum of the free hydrazone shift to 1591 and 1610 cm^{-1} in the spectrum of complex **2** and to 1588 cm^{-1} in the spectrum of complex **3**, indicating coordination of the azomethine nitrogen.[43] In complex **1**, the broad and strong band was found at 1599 cm^{-1}, in accordance with the presence of a ν(N═C) vibration, due to the formation of a new N═C bond upon coordination with deprotonation of the hydrazone ligand. Similar variations were observed for dysprosium(III) complexes of the H_2L_3 ligand (Scheme 1).[22]

Magnetic Properties. Direct-current (dc) magnetic susceptibility studies of **1**−**3** have been carried out in an applied magnetic field of 1000 Oe in the temperature range 300−2 K. The plot of $\chi_M T$ versus T, where χ_M is the molar magnetic susceptibility, is shown in Figure 6. The observed $\chi_M T$ values at 300 K are 27.3, 28.1, and 27.4 cm^3 K mol^{-1} for **1**−**3**, respectively, which are in good agreement with the expected value of 28.34 cm^3 K mol^{-1} for two uncoupled dysprosium(III) ions ($S = {}^5/_2$, $L = 5$, $^6H_{15/2}$, and $g = {}^4/_3$). The temperature dependence of the magnetic susceptibilities for all compounds shows different thermal evolution. For **3**, the $\chi_M T$ product begins a very slow decrease at higher temperatures, with the rate of decrease becoming steadily larger below 90 K and then further decreasing sharply to reach a minimum of 15.6 cm^3 K mol^{-1} at 2 K. The Stark sublevels of

dx.doi.org/10.1021/ic2014978 |*Inorg. Chem.* 2011, 50, 9705–9713

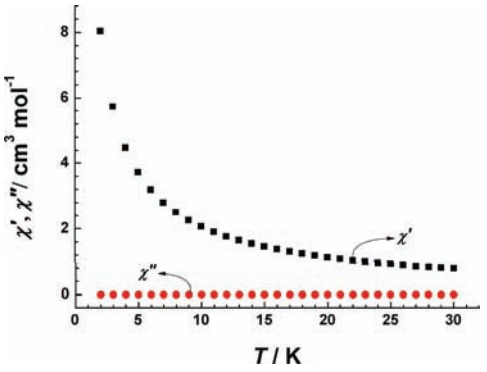

Figure 7. Temperature dependence of the in-phase (χ') and out-of-phase (χ'') ac susceptibility for **3** under zero dc field at 1000 Hz.

the anisotropic dysprosium(III) ions are thermally depopulated when the temperature is lowered, resulting in a decrease of the $\chi_M T$ value.[44,45] It is thus likely that this thermal behavior is associated with the thermal depopulation of the dysprosium(III) excited states and that Dy···Dy interactions are insignificant by comparison in **3**.[33] However, the $\chi_M T$ product for **1** gradually decreases with the temperature to reach a minimum of 25.3 cm^3 K mol^{-1} at about 26 K and then increases sharply to a maximum value of 33.9 cm^3 K mol^{-1} at 2 K, while for complex **2**, $\chi_M T$ increases only slightly to 23.7 cm^3 K mol^{-1} at 2 K after reaching a minimum value of 22.5 cm^3 K mol^{-1} at 6 K. These behaviors account for the competition between thermal depopulation of the dysprosium(III) excited states and ferromagnetic interaction within complexes **1** and **2**.

Magnetization (M) data for **1** and **2** were collected in the 0−70 kOe field range below 5 K. The nonsuperimposition of the M versus H/T data on a single mastercurve (Figures S3 and S4 in the Supporting Information) suggests the presence of magnetic anisotropy and/or the lack of a well-defined ground state, where the low-lying excited states might be populated when a field is applied.[46] The magnetization eventually reaches the value of 13.7 μ_B for **1** (10.5 μ_B for **2**) at 2 K and 70 kOe. This value is much lower than the theoretical value for two noninteracting dysprosium(III) ions [$g_J \times J = {}^4/_3 \times {}^{15}/_2 = 10\ \mu_B$ per dysprosium(III)], most likely due to the crystal-field effect at the dysprosium(III) ion, which eliminates the 16-fold degeneracy of the $^6H_{15/2}$ ground state.[47] Especially, a residual slope is observed for complex **2** at high field (>60 kOe), indicating failure of the magnetization to saturate and some anisotropy in the system (Figure S5 in the Supporting Information).

ac susceptibility measurements were carried out for **1**−**3** under a zero dc field to investigate the dynamics of magnetization. As shown in Figure 7, complex **3** does not exhibit any out-of-phase ac signal. On the contrary, both in-phase (χ') and out-of-phase (χ'') susceptibilities for **1** show the frequency dependence maximum, signaling the "freezing" of the spins by the anisotropy barriers, typical features associated with SMM behavior (Figure 8, left). However, the peaks can only be found at frequencies higher than 100 Hz. Upon cooling, increases of χ' and χ'' are observed below 5 K, indicating that blocking is not complete and thermally activated spin reversal is gradually replaced by a quantum tunneling mechanism at zero dc field.

From frequency dependencies of the ac susceptibility (Figure 8, right), the magnetization relaxation time (τ) has been estimated

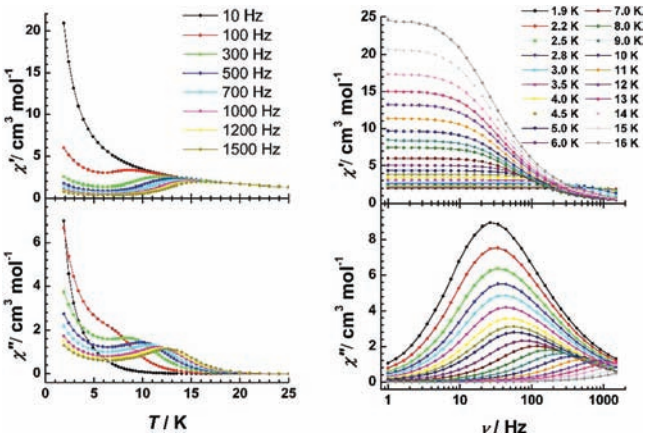

Figure 8. Temperature (left) and frequency (right) dependence of the ac susceptibility for **1** as a function of the temperature below 25 K (left) and the ac frequency between 10 and 1500 Hz (right) under a zero dc field.

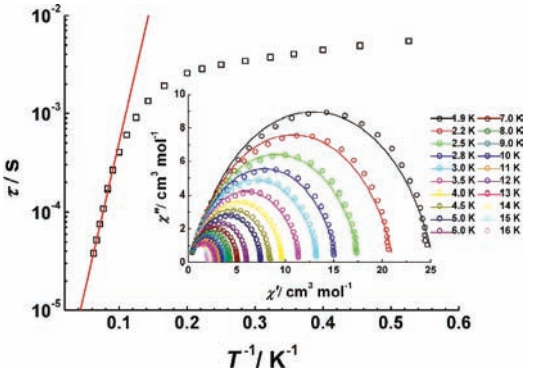

Figure 9. Magnetization relaxation time, τ, versus T^{-1} plot for **1** under a zero dc field. The solid line is fitted with the Arrhenius law. Inset: Cole−Cole plots measured at 1.9−15 K in a zero dc field. The solid lines are the best fits to the experimental data, obtained with the generalized Debye model with α parameters below 0.2.

between 1.9 and 16 K (Figure 9). Above 11 K, the relaxation follows a thermally activated mechanism, affording an energy barrier of 69 K with a preexponential factor (τ_0) of 5.3×10^{-7} s based on the Arrhenius law [$\tau = \tau_0 \exp(U_{eff}/kT)$], which is consistent with the expected τ_0 of 10^{-6}−10^{-11} for a SMM.[1] It is worth noticing that log τ becomes weakly dependent on T (more specifically $1/\tau \propto T$) as the temperature is decreased. This behavior characterizes a crossover from a thermally activated Orbach mechanism that is predominant at high temperature to a direct or phonon-induced tunneling process taking over at $T < 11$ K.[48] The data plotted as Cole−Cole plots (inset of Figure 9) show a relatively symmetrical shape and can be fitted to the generalized Debye model,[49,50] with α parameters below 0.20 ($\alpha = 0$ for a Debye model; Table S2 in the Supporting Information). This result indicates that a single relaxation time is mainly involved in the present relaxation process independently of the temperature.

The dynamics of magnetization for **2** were also investigated from ac susceptibility measurements, in a zero static field at the indicated frequencies given in Figure 10. The χ'' component of the susceptibility has a strong frequency dependence below 5 K

dx.doi.org/10.1021/ic2014978 |Inorg. Chem. 2011, 50, 9705–9713

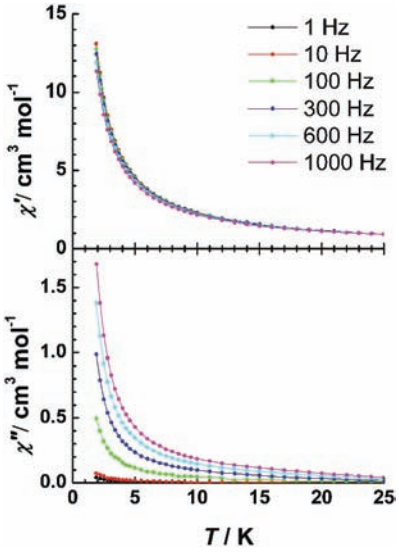

Figure 10. Temperature dependence of the in-phase (top) and out-of-phase (bottom) ac susceptibility for **2** under a zero dc field.

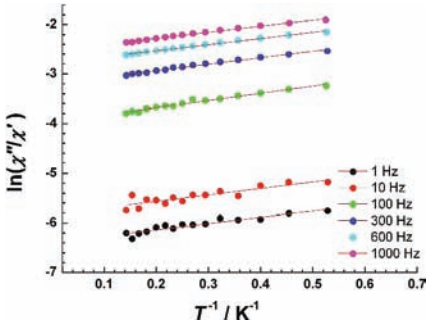

Figure 11. Natural logarithm of the ratio of χ'' over χ' versus $1/T$ of the data for **2** given in Figure 10. Slope corresponding to energy barrier U_{eff} = 1.3 K.

down to the lowest measured temperature 1.9 K, indicating the onset of slow magnetization relaxation and, thus, probable SMM behavior. Unluckily, the expected maximum due to blocking could not be observed down to this temperature. To determine the energy barrier U_{eff} and τ_0, another method, recently employed by Bartolomé et al., is to assume that there is only one characteristic relaxation process of the Debye type with one energy barrier and one time constant. With this assumption, one obtains the following relation (eq):

$$\ln(\chi''/\chi') = \ln(\omega\tau_0) + U_{eff}/kT$$

which allows one to roughly evaluate U_{eff} and τ_0. This methodology had been applied earlier in the determination of Mn_{12} acetate.[51] As shown in Figure 11, by fitting the experimental χ''/χ' data to eq , the parameter values $U_{eff} \approx 1.3$ K and $\tau_0 \approx 10^{-5}$ s were obtained. These values coincide with the relaxation time deduced from the whole set of χ'' versus frequency curves between 1.9 and 2.5 K (Figure S6 in the Supporting Information), which afford the Arrhenius plot in Figure S7 in the Supporting Information with an energy gap of 1 K and τ_0 of about 3.3×10^{-5} s. A more precise result must wait for very low temperature measurements.

Structure−Property Relationship. It has been increasingly identified in dysprosium compounds that the contribution to the barrier blocking magnetization arises mainly from blockage of the individual lanthanide centers for polynuclear SMMs[23,52,53] because the magnetic coupling between dysprosium(III) centers is expected to be very weak owing to the limited radial extension of the 4f orbitals.[54] Thus, for a weakly coupled system, the magnetic axiality of the ground Kramers doublet of a single ion plays a key role for the SMM performance of lanthanide complexes.[55,56] The versatility of the coordination of H_2**ovph** to dysprosium(III) has been shown by the formation of **1**−**3** under different reaction conditions (Scheme 2). The base strength will influence the keto−enol tautomerism and deprotonation of the H_2**ovph** ligand, resulting in distinct coordination modes to dysprosium(III) centers. Thus, the different magnetic relaxation behaviors among **1**−**3** are probably the result of different coordination geometries, which are likely to affect the nature or directions of the easy axes through the ligand fields.[57] First, complex **1** has a local hula-hoop-like geometry close to that reported for Dy_2 SMM $[Dy_2(L_3)_2(NO_3)_2(MeOH)_2]$[22] [$H_2L_3$ = (2-hydroxy-3-methoxyphenyl)methylene(isonicotino)hydrazine; Scheme 1], indicating that such a geometry may be a suitable and robust ligand field for slow magnetic relaxation on dysprosium(III) ions. Second, the relative positioning of the different strong oxygen and nitrogen donor atoms might influence the emergence of magnetic anisotropy. For example, the phenoxido oxygen atoms create very short Dy−O bonds in complexes **1** [Dy1−O2 = 2.179(4) Å] and **2** [Dy1−O2 = 2.189(6) Å], and it confirmed the formation of a strong ligand field on the local dysprosium(III) sites. In complex **3**, however, the Dy−O/N bonds uniformly distribute between 2.321(4) and 2.543(6) Å for Dy1 and between 2.314(4) and 2.516(6) Å for Dy2.

In addition, the exchange interaction between the lanthanide ions is also expected to contribute to the relaxation.[52,53] At low enough temperature, blockage of magnetization due to exchange interaction between the metal sites in the weak exchange limit has been observed in several dysprosium-based SMMs.[30,58,59] It is worth noting that the magnetic interactions are drastically different among **1**−**3**, as shown in Figure 6. These interaction differences might generate dissimilar anisotropy of lowest exchange multiplets, therefore affecting the dynamic magnetic behavior.

Indeed, no obvious magnetic coupling between dysprosium(III) centers is noticed for compound **3**, while a ferromagnetic interaction was clearly observed within complexes **1** and **2** at low temperatures (Figure 6). These distinct magnetic behaviors must be caused by crucial structural differences between the $[Dy_2(\mu\text{-O})_2]$ (**1** and **2**) and $[Dy_2(\mu\text{-O})_3]$ (**3**) cores. As evidenced in Table 3, the Dy−O−Dy angles in both **1** and **2** are larger than 110°. However, in compound **3**, the resulting Dy−O−Dy angles vary from only 92.14 to 100.08°, which are more than 10° smaller than those observed in **1** and **2**, probably induced by the presence of additional μ-OH^- bridges. The main, significant disparities between the three Dy_2 cores are thus found in the Dy−O−Dy angles. Therefore, different magnetic interactions between the metal centers induced by the μ-O bridges will be another important factor for the distinct magnetic dynamics observed for compounds **1**−**3**.[60,61] It is well-known for other metal ions linked by μ-O ligands that the M−O−M angles have a great influence on the magnetic exchange coupling.[62−66] One can rationally expect the same effect for the Dy−O−Dy angles. Indeed, the Dy−O−Dy angle will modify the overlap between the magnetic orbitals of the dysprosium ions and therefore will

dx.doi.org/10.1021/ic2014978 |Inorg. Chem. 2011, 50, 9705–9713

influence the intradinuclear magnetic interactions (Figure 6), although such interactions are expected to be very weak. These features clearly suggest that the strength of the local crystal field modulated by the versatile H_2**ovph** ligand, together with the exchange interactions between them induced by the μ-O bridges, is responsible for the different magnetic behaviors observed.

In complex **1**, the **ovph**$^{2-}$ ligand has the capability not only of holding a suitable crystal field on the local dysprosium sites but also of promoting magnetic interactions. Accordingly, such a complex can be regarded as a lanthanide SMM building block, which can be used for the design of more efficient polynuclear SMMs. Recent work indicates that the replacement of the auxiliary ligands in complex **1** may suppress their zero-field tunneling of magnetization.[67] Further work to prepare and investigate increasingly larger cluster compounds based on the magnetic building blocks of **1** is currently in progress.

CONCLUSION

Three dinuclear dysprosium(III) complexes have been assembled using the versatile H_2**ovph** ligand. The aroylhydrazone ligands form different coordination modes in three title complexes (Scheme 2) because of their tautomeric maneuver, depending on the reaction conditions. The structural differences (induced by the different coordination modes in **1**−**3**) clearly affect the orbital overlaps between the metal centers and ligands, as well as the local tensor of anisotropy on each dysprosium site and their relative orientations, therefore generating dissimilar dynamic magnetic behavior; namely, compounds **1** and **2** show SMM behavior, while compound **3** does not display slow relaxation of magnetization. Theoretical studies are required to thoroughly analyze the Dy−O−Dy angle/magnetic property relationship. The present results demonstrate that suitable crystal fields on the dysprosium sites may lead to an efficient blocking of magnetization. This provides a promising strategy for enhancing the SMM properties of polynuclear lanthanide-based complexes via fine-tuning of the local environments of the lanthanide ions.

ASSOCIATED CONTENT

Supporting Information. Tables of hydrogen bonds (Table S1) and relaxation fitting parameters (Table S2) and figures of crystal structures (Figures S1 and S2) and magnetic measurements (Figures S3−S7). This material is available free of charge via the Internet at http://pubs.acs.org.

AUTHOR INFORMATION

Corresponding Author
*E-mail: tang@ciac.jl.cn.

ACKNOWLEDGMENT

We thank the National Natural Science Foundation of China (Grants 20871113, 91022009, and 20921002) for its financial support.

REFERENCES

(1) Gatteschi, D.; Sessoli, R.; Villain, J. *Molecular Nanomagnets*; Oxford University Press: Oxford, U.K., 2006.
(2) Sessoli, R.; Gatteschi, D.; Caneschi, A.; Novak, M. A. *Nature* **1993**, *365*, 141.
(3) Gatteschi, D.; Sessoli, R. *Angew. Chem., Int. Ed.* **2003**, *42*, 268.
(4) Gatteschi, D.; Caneschi, A.; Pardi, L.; Sessoli, R. *Science* **1994**, *265*, 1054.
(5) Sessoli, R.; Tsai, H. L.; Schake, A. R.; Wang, S.; Vincent, J. B.; Folting, K.; Gatteschi, D.; Christou, G.; Hendrickson, D. N. *J. Am. Chem. Soc.* **1993**, *115*, 1804.
(6) Leuenberger, M. N.; Loss, D. *Nature* **2001**, *410*, 789.
(7) Hill, S.; Edwards, R. S.; Aliaga-Alcalde, N.; Christou, G. *Science* **2003**, *302*, 1015.
(8) Bogani, L.; Wernsdorfer, W. *Nat. Mater.* **2008**, *7*, 179.
(9) Urdampilleta, M.; Klyatskaya, S.; Cleuziou, J. P.; Ruben, M.; Wernsdorfer, W. *Nat. Mater.* **2011**, *10*, 502.
(10) Aromí, G.; Brechin, E. K. *Struct. Bonding (Berlin)* **2006**, *122*, 1.
(11) Sessoli, R.; Powell, A. K. *Coord. Chem. Rev.* **2009**, *253*, 2328.
(12) Lin, S.-Y.; Guo, Y.-N.; Xu, G.-F.; Tang, J. *Chin. J. Appl. Chem.* **2010**, *27*, 1365.
(13) Guo, Y.-N.; Xu, G.-F.; Guo, Y.; Tang, J. *Dalton Trans.* **2011**, DOI: 10.1039/C1DT10474H.
(14) Ishikawa, N.; Sugita, M.; Ishikawa, T.; Koshihara, S.-y.; Kaizu, Y. *J. Am. Chem. Soc.* **2003**, *125*, 8694.
(15) Ishikawa, N. *J. Phys. Chem. A* **2003**, *107*, 5831.
(16) Kajiwara, T.; Takahashi, K.; Hiraizumi, T.; Takaishi, S.; Yamashita, M. *CrystEngComm* **2009**, *11*, 2110.
(17) Sorace, L.; Benelli, C.; Gatteschi, D. *Chem. Soc. Rev.* **2011**, *40*, 3092.
(18) Ishikawa, N.; Sugita, M.; Wernsdorfer, W. *J. Am. Chem. Soc.* **2005**, *127*, 3650.
(19) AlDamen, M. A.; Clemente-Juan, J. M.; Coronado, E.; Martí-Gastaldo, C.; Gaita-Arino, A. *J. Am. Chem. Soc.* **2008**, *130*, 8874.
(20) AlDamen, M. A.; Cardona-Serra, S.; Clemente-Juan, J. M.; Coronado, E.; Gaita-Ariño, A.; Martí-Gastaldo, C.; Luis, F.; Montero, O. *Inorg. Chem.* **2009**, *48*, 3467.
(21) Luis, F.; Martínez-Pérez, M. J.; Montero, O.; Coronado, E.; Cardona-Serra, S.; Martí-Gastaldo, C.; Clemente-Juan, J. M.; Sesé, J.; Drung, D.; Schurig, T. *Phys. Rev. B* **2010**, *82*, 060403.
(22) Lin, P. H.; Burchell, T. J.; Clérac, R.; Murugesu, M. *Angew. Chem., Int. Ed.* **2008**, *47*, 8848.
(23) Lin, P. H.; Burchell, T. J.; Ungur, L.; Chibotaru, L. F.; Wernsdorfer, W.; Murugesu, M. *Angew. Chem., Int. Ed.* **2009**, *48*, 9489.
(24) Guo, Y.-N.; Xu, G.-F.; Gamez, P.; Zhao, L.; Lin, S.-Y.; Deng, R.; Tang, J.; Zhang, H.-J. *J. Am. Chem. Soc.* **2010**, *132*, 8538.
(25) Hewitt, I. J.; Tang, J.; Madhu, N. T.; Anson, C. E.; Lan, Y.; Luzon, J.; Etienne, M.; Sessoli, R.; Powell, A. K. *Angew. Chem., Int. Ed.* **2010**, *49*, 6352.
(26) Blagg, R. J.; Muryn, C. A.; McInnes, E. J. L.; Tuna, F.; Winpenny, R. E. P. *Angew. Chem., Int. Ed.* **2011**, *50*, 6530.
(27) Rinehart, J. D.; Fang, M.; Evans, W. J.; Long, J. R. *Nat. Chem.* **2011**, *3*, 538.
(28) Rinehart, J. D.; Meihaus, K. R.; Long, J. R. *J. Am. Chem. Soc.* **2010**, *132*, 7572.
(29) Tang, J.; Hewitt, I.; Madhu, N. T.; Chastanet, G.; Wernsdorfer, W.; Anson, C. E.; Benelli, C.; Sessoli, R.; Powell, A. K. *Angew. Chem., Int. Ed.* **2006**, *45*, 1729.
(30) Luzon, J.; Bernot, K.; Hewitt, I. J.; Anson, C. E.; Powell, A. K.; Sessoli, R. *Phys. Rev. Lett.* **2008**, *100*, 247205.
(31) Chibotaru, L. F.; Ungur, L.; Soncini, A. *Angew. Chem., Int. Ed.* **2008**, *47*, 4126.
(32) Car, P.-E.; Perfetti, M.; Mannini, M.; Favre, A.; Caneschi, A.; Sessoli, R. *Chem. Commun.* **2011**, *47*, 3751.
(33) Abbas, G.; Lan, Y.; Kostakis, G. E.; Wernsdorfer, W.; Anson, C. E.; Powell, A. K. *Inorg. Chem.* **2010**, *49*, 8067.
(34) Li, S.-H.; Gao, S.-K.; Liu, S.-X.; Guo, Y.-N. *Cryst. Growth Des.* **2010**, *10*, 495.
(35) Yu, G. M.; Li, Y. H.; Zou, L. F.; Zhu, J. W.; Liu, X. Q. *Acta Crystallogr., Sect. E* **2010**, *66*, M693.
(36) Yu, G. M.; Zhao, L.; Guo, Y. N.; Xu, G. F.; Zou, L. F.; Tang, J. K.; Li, Y. H. *J. Mol. Struct.* **2010**, *982*, 139.
(37) Sheldrick, G. M. *SHELXS-97, Program for Crystal Structure Solution*; University of Göttingen: Göttingen, Germany, 1997.

(38) Wang, D.; Liu, S. X. *Polyhedron* **2007**, *26*, 5469.
(39) Runschke, C.; Meyer, G. *Z. Anorg. Allg. Chem.* **1997**, *623*, 1493.
(40) Ruiz-Martinez, A.; Casanova, D.; Alvarez, S. *Chem.—Eur. J.* **2008**, *14*, 1291.
(41) Matoga, D.; Szklarzewicz, J.; Stadnicka, K.; Shongwe, M. S. *Inorg. Chem.* **2007**, *46*, 9042.
(42) Perez-Rebolledo, A.; Piro, O. E.; Castellano, E. E.; Teixeira, L. R.; Batista, A. A.; Beraldo, H. *J. Mol. Struct.* **2006**, *794*, 18.
(43) Despaigne, A. A. R.; da Silva, J. G.; do Carmo, A. C. M.; Sives, F.; Piro, O. E.; Castellano, E. E.; Beraldo, H. *Polyhedron* **2009**, *28*, 3797.
(44) Kahn, M. L.; Ballou, R.; Porcher, P.; Kahn, O.; Sutter, J. P. *Chem.—Eur. J.* **2002**, *8*, 525.
(45) Kahn, M. L.; Sutter, J. P.; Golhen, S.; Guionneau, P.; Ouahab, L.; Kahn, O.; Chasseau, D. *J. Am. Chem. Soc.* **2000**, *122*, 3413.
(46) Abbas, G.; Lan, Y. H.; Kostakis, G.; Anson, C. E.; Powell, A. K. *Inorg. Chim. Acta* **2008**, *361*, 3494.
(47) Osa, S.; Kido, T.; Matsumoto, N.; Re, N.; Pochaba, A.; Mrozinski, J. *J. Am. Chem. Soc.* **2004**, *126*, 420.
(48) Gonidec, M.; Luis, F.; Vílchez, À.; Esquena, J.; Amabilino, D. B.; Veciana, J. *Angew. Chem., Int. Ed.* **2010**, *49*, 1623.
(49) Cole, K. S.; Cole, R. H. *J. Chem. Phys.* **1941**, *9*, 341.
(50) Aubin, S. M. J.; Sun, Z.; Pardi, L.; Krzystek, J.; Folting, K.; Brunel, L.-C.; Rheingold, A. L.; Christou, G.; Hendrickson, D. N. *Inorg. Chem.* **1999**, *38*, 5329.
(51) Luis, F.; Bartolome, J.; Fernandez, J. F.; Tejada, J.; Hernandez, J. M.; Zhang, X. X.; Ziolo, R. *Phys. Rev. B* **1997**, *55*, 11448.
(52) Layfield, R. A.; McDouall, J. J. W.; Sulway, S. A.; Tuna, F.; Collison, D.; Winpenny, R. E. P. *Chem.—Eur. J.* **2010**, *16*, 4442.
(53) Wang, Y.; Li, X.-L.; Wang, T.-W.; Song, Y.; You, X.-Z. *Inorg. Chem.* **2010**, *49*, 969.
(54) Mazzanti, M. *Nat. Chem.* **2011**, *3*, 426.
(55) Feltham, H. L. C.; Lan, Y.; Klöwer, F.; Ungur, L.; Chibotaru, L. F.; Powell, A. K.; Brooker, S. *Chem.—Eur. J.* **2011**, *17*, 4362.
(56) Watanabe, A.; Yamashita, A.; Nakano, M.; Yamamura, T.; Kajiwara, T. *Chem.—Eur. J.* **2011**, *17*, 7428.
(57) Yang, P.-P.; Gao, X.-F.; Song, H.-B.; Zhang, S.; Mei, X.-L.; Li, L.-C.; Liao, D.-Z. *Inorg. Chem.* **2011**, *50*, 720.
(58) Long, J.; Habib, F.; Lin, P.-H.; Korobkov, I.; Enright, G.; Ungur, L.; Wernsdorfer, W.; Chibotaru, L. F.; Murugesu, M. *J. Am. Chem. Soc.* **2011**, *133*, 5319.
(59) Lin, P.-H.; Korobkov, I.; Wernsdorfer, W.; Ungur, L.; Chibotaru, L. F.; Murugesu, M. *Eur. J. Inorg. Chem.* **2011**, 1535.
(60) Ke, H.; Gamez, P.; Zhao, L.; Xu, G.-F.; Xue, S.; Tang, J. *Inorg. Chem.* **2010**, *49*, 7549.
(61) Gao, Y. J.; Xu, G. F.; Zhao, L.; Tang, J.; Liu, Z. L. *Inorg. Chem.* **2009**, *48*, 11495.
(62) Ruiz, E.; Alemany, P.; Alvarez, S.; Cano, J. *Inorg. Chem.* **1997**, *36*, 3683.
(63) Ruiz, E.; Alemany, P.; Alvarez, S.; Cano, J. *J. Am. Chem. Soc.* **1997**, *119*, 1297.
(64) Cañada-Vilalta, C.; O'Brien, T. A.; Brechin, E. K.; Pink, M.; Davidson, E. R.; Christou, G. *Inorg. Chem.* **2004**, *43*, 5505.
(65) Crawford, V. H.; Richardson, H. W.; Wasson, J. R.; Hodgson, D. J.; Hatfield, W. E. *Inorg. Chem.* **1976**, *15*, 2107.
(66) Merz, L.; Haase, W. *J. Chem. Soc., Dalton Trans.* **1980**, 875.
(67) Guo, Y.-N.; Xu, G.-F.; Wernsdorfer, W.; Ungur, L.; Guo, Y.; Tang, J.; Zhang, H.; Chibotaru, L. F.; Powell, A. K. *J. Am. Chem. Soc.* **2011**, *133*, 11948.